Mon. Not. R. astr. Soc. (1991) **253,** 107–122 and *Microfiche MN 253/1*

Atoms in very strong magnetic fields

M. C. Miller[1,2]★ and D. Neuhauser[3]

[1] *Theoretical Astrophysics, California Institute of Technology, Pasadena, California 91125 USA*
[2] *High Energy Physics, University of Illinois at Urbana-Champaign, Urbana, Illinois 61801, USA*
[3] *W. K. Kellogg Radiation Laboratory, California Institute of Technology, Pasadena, California 91125 USA*

Accepted 1991 June 14. Received 1991 June 5; in original form 1990 September 14

SUMMARY

The X-ray spectra of neutron stars are expected to be determined by the opacities of atoms with atomic number $Z>2$ in strong magnetic fields. We calculate the energy levels, wavefunctions and transition rates of hydrogen, helium, carbon, nitrogen and silicon in the very strong ($B>4.7\times10^9Z^2$ G) magnetic fields expected in neutron stars. The wavefunctions are represented in terms of Landau states, and are calculated with a high-field multiconfigurational Hartree–Fock code. We compare our results for hydrogen with previous work and use our wavefunctions to compute bound–bound and bound–free oscillator strengths for heavier elements. The accuracy of our method is sufficient for the applications we make of it in a companion paper (Miller 1991), where we compute neutron star thermal X-ray spectra. The low fluxes expected from such objects ($<10^{-11}$ erg cm^{-2} s^{-1} from thermal X-rays) imply that the appropriate wavefunctions and energy levels need only be calculated with an accuracy of a few per cent. There are other methods in the literature which give a higher accuracy (which we do not need in the present context) for hydrogen. However, unlike these other methods, our method can be readily extended, with calibrated accuracy, to elements of higher Z, as we show in the present paper.

1 INTRODUCTION

The existence of sensitive, imaging X-ray satellites has made the detection of thermal flux from neutron stars a realistic possibility. Recent research (see Tsuruta 1986 for a review) has indicated that the effective surface temperature of neutron stars should remain above $\approx10^5$ K $=10$ eV for 10^5 yr, barring the presence of pion condensates or other exotic matter. The star should remain a detectable X-ray source during that period. While white dwarfs have magnetic fields B small enough ($B<5\times10^8$ G) that energy levels may be computed by perturbation theory (Zeeman splittings) with errors of <2 per cent, observed neutron stars typically have fields in the range of 10^9 to 5×10^{12} G (Taylor & Stinebring 1986; Joss & Rappaport 1984), so that the magnetic interaction may no longer be treated as a perturbation, and atomic structure is drastically changed, modifying the opacity. While the changes in the opacity will not change the total energy radiated (Hernquist 1985), they will result in a redistribution of the emergent power among frequencies (see, e.g. Mihalas 1978). This redistribution affects the flux in the bandpasses of different detectors differently, and may give rise to detectable spectral features. Work has been done (Romani 1987) on radiative transfer in neutron star atmospheres, but this work has used opacity tables computed for $B=0$.

A prerequisite to further work on predictions and interpretations of X-ray spectra of neutron stars is accurate atomic data for atoms in strong magnetic fields. In recent years, much research has been done (Simola & Virtamo 1978; O'Connell 1979; Kara & McDowell 1980; Wunner *et al.* 1981; Rösner *et al.* 1983; Rösner *et al.* 1984; Forster *et al.* 1984; Ruder *et al.* 1985; Wunner 1986; Wunner & Ruder 1987; Wunner, Geyer & Ruder 1987) on the properties of hydrogen in very large magnetic fields. However, comparatively little has been done on helium or other elements, which could be important in determining the spectrum. Current models of supernovae indicate that the mass cut should occur within the iron layer. However, it is possible that significant amounts of nickel or other heavy elements could be produced by the shock wave from the supernova, and in the event of an asymmetrical explosion, the neutron star could accrete large amounts of any of the elements in the fusion chain. An optical depth of unity in X-rays occurs at a depth of only ≈1 cm, which at a density of 1 g cm^{-3} is only $\approx10^{13}$ g $\approx10^{-20}M_\odot$

★ Current address: High Energy Physics, University of Illinois at Urbana-Champaign, Urbana, Illinos 61801 USA.

over the surface of the neutron star, so the very top layer of the atmosphere will dominate the opacity. Since the surface gravity is so high, gravitational separation will be very rapid, on the order of $\sim 1-100$ s for a helium photosphere of typical temperature and density (Alcock & Illarionov 1980), and the lightest element present will rise to the top. A similar situation occurs in white dwarfs (Liebert 1980), where stars with virtually pure hydrogen and helium atmospheres have been detected. Another factor is that if the column depth of, e.g., hydrogen becomes large enough, nuclear reactions may convert it to helium, and so on. For an overview of these processes, see Shapiro & Teukolsky 1983 Chapter 3 Section 7.

The conclusion is that since the surface of observable neutron stars could have almost any composition (elements heavier than helium being perhaps the most likely in isolated neutron stars), we should investigate many possibilities. Astrophysical calculations ultimately need X-ray opacity tables similar to the zero-field tables in Saloman, Hubbell & Scofield 1988, but as a function of B from 0 to 10^{13} Gauss. This paper is a first step in the production of such opacity tables. It is important to stress that the only objects believed to have magnetic fields in the 10^{10}–10^{13} G range are neutron stars, and that the thermal X-ray emission from these objects has extremely low flux. Even the Crab pulsar, with a predicted surface temperature of $\approx 10^6$ K and a distance of $d \gtrsim 1$ kpc, would only be expected to produce $\lesssim 30$ thermal photons per second observable by *ROSAT* (which has a collecting area of ≈ 1000 cm^2), so detailed spectra will be difficult to establish. Furthermore, the magnetic field is expected to have a large gradient over the surface of the star ($\sim$ factor of 2). As can be seen in detail in Sections 3 and 4, such a large change in magnetic field can affect strongly the energies of spectral features; for example, the ground state binding energy of hydrogen varies from roughly 160 eV at 10^{12} G to about 200 eV at 2×10^{12} G. Another obstacle to detailed analysis of spectra is that our knowledge of the neutron star equation of state is still fairly crude. Current equations of state predict surface gravitational redshifts ranging between $z = 1.1$ and 1.2, so there is a built-in uncertainty of ≈ 10 per cent in photon energies. Since the most optimistically envisaged X-ray satellites do not have energy resolutions exceeding a few per cent, it is unnecessary at this stage to determine energies to many significant figures, and the accuracy of the energy calculations presented here (better than 5 per cent) is more than adequate for the present purpose. Given sufficiently long integration time, it may be possible to determine observationally oscillator strengths to high accuracy, but the multitude of theoretical uncertainties make accurate prediction difficult. For the moment, about all that can be done is to get data for a first-pass calculation to see what transitions are important, and for that purpose our computations (accurate to better than 20 per cent for oscillator strengths) are perfectly acceptable. We use a multiconfigurational Hartree–Fock code as a general method for determining the energy levels and wavefunctions of any atom in very high fields, and also compute the bound–bound and bound–free transition strengths for such atoms. In Section 2, we discuss the physics of atoms in high magnetic fields and the Hartree–Fock method, and also derive the bound–bound and bound–free cross sections in a high field. In Section 3, we describe the convergence tests of our program and compare our results with previous results for hydrogen and helium. In Section 4 we present our new results for the energy levels and transition probabilities for helium and carbon.

2 METHOD

2.1 Generation of the wavefunctions

In the following sections we will use the convention that the length scale will be the Landau scale

$$\hat{\rho} = \sqrt{\frac{\hbar c}{eB}} = 2.5 \times 10^{-10} B_{12}^{-1/2} \text{ cm}, \tag{1}$$

where $B_{12} = B/10^{12}$ G, and the magnetic field will be measured in terms of the reference field

$$B_0 = \frac{2\alpha^2 m_e^2 c^2}{e\hbar} = 4.7 \times 10^9 \text{ G}, \tag{2}$$

which is the field at which the Coulomb and magnetic energies are equal for hydrogen.

The Hamiltonian of a neutral atom in a uniform magnetic field is

$$\begin{aligned} H &= H_B + V_{en} + V_{ee} \\ &= \sum_i \frac{1}{2M}\left(\boldsymbol{p}_i + \frac{e}{c}\boldsymbol{A}_i\right)^2 + \sum_i \frac{e}{mc}\boldsymbol{B}\cdot\boldsymbol{S}_i - Ze^2\sum_i \frac{1}{r_i} + e^2 \sum_{i<j} \frac{1}{r_{ij}}, \end{aligned} \tag{3}$$

where $\boldsymbol{p}_i$ is the momentum of the ith electron; $\boldsymbol{A}$ is the vector potential of a constant magnetic field, $\boldsymbol{A} = \frac{1}{2}\boldsymbol{B} \times \boldsymbol{r}$; $\boldsymbol{S}$ is the spin; Z is the atomic number; r_i is the position of the ith electron; r_{ij} is the separation between the ith and jth electrons; H_B is the single-particle magnetic Hamiltonian; V_{en} is the electron–nucleus potential and V_{ee} is the electron–electron potential.

Since we are dealing with very strong magnetic fields ($B \gg Z^2 B_0$), a cylindrical expansion

$$\Psi_{m\nu}(z, \rho, \phi) = \sum_n f_{nm\nu}(z)\, \Phi_{nm}(\rho, \phi) \tag{4}$$

will be used. The magnetic field is defined to be uniform and along the z axis, ν, m and n are, respectively, the z, ϕ (azimuthal) and ρ (radial) quantum numbers, and the Φ_{nm} are the Landau states

$$\Phi_{nm}(\rho, \phi) = \frac{\sqrt{n!}}{\sqrt{2\pi(n+|m|)!\hat{\rho}^2}} \left(\frac{\rho}{\sqrt{2}\hat{\rho}}\right)^{|m|} e^{-\rho^2/4\hat{\rho}^2} L_n^{|m|}\left(\frac{\rho^2}{2\hat{\rho}}\right) e^{-im\phi}, \tag{5}$$

where $L_n^{|m|}$ are the associated Laguerre polynomials. In this paper we will deal only with $n = 0$ states, because $n \neq 0$ states have much higher energy, on the order of the cyclotron energy $\hbar\omega_c = \hbar eB/Mc \approx 11.5\, B_{12}$ keV. Strictly speaking, this expansion is valid only for $B \gg Z^2 B_0$, but in practice (Rösner *et al.* 1984) accurate energy values may be generated for $B/Z^2 B_0 \gtrsim 1$, though near the critical field more terms ($n > 0$) need to be kept. At the critical field and below, a spherical expansion

$$\Psi_m(\boldsymbol{r}) = \sum_l \frac{1}{r} f_l(r)\, Y_{lm}(\theta, \phi)$$

should be used, and the combination of the two regimes allows the structure of atoms to be calculated in arbitrary fields. For additional comments on the validity of these methods, see Rösner *et al.* 1984.

The technique that we have chosen for determining the wavefunctions in the Hartree–Fock method, which is equivalent to solving the variational equation

$$\frac{\delta}{\delta\chi}\left(\frac{\langle\Psi|H|\Psi\rangle}{\langle\Psi|\Psi\rangle}\right) = 0, \tag{6}$$

where χ is the total wavefunction

$$\chi = \Psi|S_z\rangle,$$

$|S_z\rangle$ is the spin wavefunction, and the wavefunction Ψ is approximated by a one-particle Slater determinant.

In strong fields, the wavefunctions are approximately separable into components perpendicular to the B field ($\hat{\rho}, \hat{\phi}$) and the component parallel to the field ($\hat{z}$), with the only unknowns being the one-dimensional functions $f_{0m\nu}(z)$, so the Hartree–Fock equations reduce to the one-dimensional coupled equations

$$\frac{\delta}{\delta f_{0m\nu}(z)}\left(\frac{\langle\Psi|H|\Psi\rangle}{\langle\Psi|\Psi\rangle}\right) = 0. \tag{7}$$

For further details about the behaviour of the Hartree–Fock equations, see Froese Fischer 1977.

There has been a debate about whether a renormalization of the wavefunctions should be applied to compensate for screening effects for $B = 0$ and $Z < 55$ (Pratt 1960; Pratt & Tseng 1972). This renormalization is done by replacing the nuclear charge Z in the wavefunction with an effective charge $Z_{\rm eff}$, where $Z_{\rm eff} = Z - S$, and S is a screening parameter (e.g. $S = 0.3$ for the K shell, $S = 4.15$ for the L shell). This procedure would most greatly affect the outer shells, and would typically alter the cross section by less than 10 per cent. However, comparisons with experimental results (Saloman *et al.* 1988) indicate that the unrenormalized wavefunctions give better agreement, so we do not attempt to correct for screening effects. Besides errors that are due to truncation of the configuration space (which can be eliminated by using more powerful computers), most of the error in zero-field Hartree–Fock calculations is caused by the symmetrization of the spatial wavefunction of electrons in a spin-singlet state. In the full wavefunction, the electron–electron repulsion causes a depletion of the wavefunction for small relative distances (Coulomb hole); naive symmetrization of the orbitals causes the opposite effect. For electrons in a spin-triplet state, the antisymmetrization of the spatial wavefunction creates a hole that imitates the Coulomb hole. In strong fields, the spins are all aligned antiparallel to the field; all electron-pairs are in a spin-triplet state, and the Slater determinant reduces to a totally antisymmetric spatial determinant. The error is therefore significantly smaller than the 1 per cent error associated with zero-field calculations (Weissbluth 1978). In our program, the main source of untested error is the assumption that $n = 0$; for a comparison with the multiterm expansion of Rösner *et al.*, see Section 3.2.

In our calculations, we ignore effects associated with the finite mass of the nucleus. Inclusion of this adjustment introduces small corrections to the strengths of interactions with $\Delta m = 1$ (see Section 3.2), but for the purpose of computing neutron star

thermal spectra these corrections are insignificant. In the limit that the nucleus is infinitely massive, the expectation value of the Hamiltonian is

$$E=\langle H\rangle=\langle H_{\rm B}\rangle+\langle V_{\rm en}\rangle+\langle V_{\rm ee}\rangle, \tag{8}$$

where

$$\langle H_{\rm B}\rangle=\langle H_z\rangle=\frac{\hbar^2}{2M}\sum_{m\nu}\int|f'_{m\nu}(z)|^2\,dz \qquad \langle V_{\rm en}\rangle=-\frac{Ze^2}{\hat{\rho}}\sum_{m\nu}\int V_m(z)|f_{m\nu}(z)|^2\,dz$$

$$\langle V_{\rm ee}\rangle=\frac{e^2}{\hat{\rho}}\sum_{m\nu m'\nu'}\left(\iint D_{mm'}(z-z')|f_{m\nu}(z)|^2|f_{m'\nu'}(z')|^2-E_{mm'}(z-z')f_{m\nu}(z)f_{m'\nu'}(z')f^*_{m'\nu'}(z)f^*_{m\nu}(z')\right)dz\,dz', \tag{9}$$

with the nuclear, direct and exchange kernels

$$V_m(z)=\int\frac{|\Phi_{m0}(\rho)|^2}{\sqrt{\rho^2+z^2}}\rho\,d\rho\,d\phi=\int\frac{e^{-\rho^2/2}\rho^{2m+1}}{2^m m!\sqrt{\rho^2+z^2}}d\rho$$

$$D_{mm'}(z-z')=\int\frac{e^{-(\rho^2+\rho'^2)/2}\rho^{2m+1}\rho'^{2m'+1}}{2^{m+m'}m!m'!\sqrt{(\rho-\rho')^2+(z-z')^2}}d\rho\,d\rho'$$

$$E_{mm'}(z-z)=\int\int\int\int\frac{e^{-(\rho^2+\rho'^2)/2}(\rho\rho')^{m'+m+1}e^{-i(m-m')(\phi-\phi')}}{2^{m+m'}m!m'!\sqrt{(\rho-\rho')^2+(z-z')^2}}d\rho\,d\rho'\frac{d\phi}{2\pi}\frac{d\phi'}{2\pi},$$

and we used the fact that for the $n=0$ orbitals, $\langle H_z\rangle=-\langle H_\perp\rangle$. The Hartree–Fock equation (6) for the ground-state orbitals are equivalent to

$$\frac{\delta\langle\Psi|H|\Psi\rangle}{\delta f^*_{m\nu}(z)}=\varepsilon_{m\nu}\frac{\delta\langle\Psi|\Psi\rangle}{\delta f^*_{m\nu}(z)}, \tag{10}$$

where the Lagrange multipliers, $(\varepsilon_{m\nu})$, ensuring the orthogonality relations, are the single particle energies. It can be shown that these equations are

$$\left[-\frac{\hbar^2}{2M}\frac{d^2}{dz^2}-\frac{Ze^2}{\hat{\rho}}V_m(z)+\frac{e^2}{\hat{\rho}}K_m(z)-\varepsilon_{m\nu}\right]f_{m\nu}(z)=\frac{e^2}{\hat{\rho}}J_{m\nu}(z), \tag{11}$$

where

$$K_m(z)\equiv\sum_{m'\nu'}\int D_{mm'}(z-z')|f_{m'\nu'}|^2\,dz', \qquad J_{m\nu}(z)\equiv\sum_{m'\nu'}f_{m'\nu'}(z)\int E_{mm'}(z-z')f^*_{m'\nu'}(z')f_{m\nu}(z')\,dz'. \tag{12}$$

The initial wavefunctions, taken from restricted variational studies (Flowers *et al.* 1977; Lee 1976), were of the form

$$f_{m\nu}\propto z^\nu e^{-a_{m\nu}|z|/\hat{\rho}}. \tag{13}$$

In this equation, the coefficients $a_{m\nu}\approx 1$ (see Lee 1976 for a table of values), but the final solution is insensitive to wide variation in the parameters. These wavefunctions are generated for all of the states of interest, then equation (11) is solved for the new wavefunctions, which are orthonormalized, and the procedure is repeated until the total energy (8) converges. The orthonormalization property,

$$\iiint\Psi^*_{nm\nu}(z,\rho,\phi)\,\Psi_{n'm'\nu'}(z,\rho,\phi)\,\rho\,d\rho\,d\phi\,dz=\delta_{nn'}\delta_{mm'}\delta_{\nu\nu'}, \tag{14}$$

is guaranteed for states of different n or m by the properties of the Landau function (5), while for states of different ν the Gram–Schmidt procedure is used.

The program may be represented in algorithm form as follows.

(i) Take a set of quantum numbers, $\{m\nu\}$, large enough to include those of all occupied states.
(ii) Guess the wavefunctions, f, and guess which states are occupied.
(iii) From (12) and the wavefunctions of the occupied states, obtain the integrals $(K_m, J_{m\nu})$.
(iv) Calculate the total energy (8).
(v) Calculate the single particle energies by taking the scalar products of equation (11) with the wavefunctions $f_{m\nu}$. The Z states with the lowest energy will be the occupied states.
(vi) With the kernels and the single-particle energies, solve (11) for the new wavefunctions. With K and J, the equations are uncoupled and inhomogeneous; they are easily solved by the Green's function method (Koonin 1986).
(vii) Orthonormalize the new wavefunctions.
(viii) Iterate (iii–vii) until the total energy converges.

This algorithm will produce the ground state of the atom; it is also possible to generate any excited state by specifying that state as occupied.

In addition to the initial wavefunction, the program accepts as input the length of the integration box L (in units of $\hat{\rho}$) and the number of integration points N.

The ground state orbitals are the Z states with the lowest energy, and as a general rule states with $(m=0,\ldots,Z-1;\nu=0)$ will be occupied. For example, for $B_{12}=1$ and $Z\leq 12$, there are no occupied states with $\nu>0$, though for iron $(Z=26)$, $m=0$ through $m=5$ and $\nu=1$ are all occupied. For $B_{12}=5$, and $Z<19$, $\nu>0$ states are unoccupied, while for $Z=26$, $m=0$ and 1 with $\nu=1$ are occupied. We can understand this preference for $\nu=0$ states qualitatively by replacing the probability distribution of the electrons with that of a long cylinder with radius $\hat{\rho}$ and length l (Ruderman 1971), so the energy is roughly

$$E\approx\frac{\hbar^2}{2Ml^2}-\frac{Ze^2}{l}\log\left(\frac{l}{\hat{\rho}}\right) \tag{15}$$

and minimization with respect to l yields

$$l=l_g\approx\left[\frac{a_0/Z\hat{\rho}}{\log(a_0/Z\hat{\rho})}\right]\hat{\rho} \tag{16}$$

for the ground state, where a_0 is the Bohr radius, $a_0=0.5\times10^{-8}$ cm. For a state $\nu>0$, the typical distance from the nucleus to the electron is greater than l_g, so the binding energy is $|E|\leq Ze^2/l_g$. For a state with $m>0$, the dependence of E on ρ is logarithmic, so the energy is almost unchanged and $m>0$ states have lower energy than $\nu>0$ states. Further details are contained in Neuhauser (1986).

2.2 Transition strengths and cross sections

The radiative transitions of hydrogen have been treated in great detail in, e.g. Forster *et al.* 1984, and a good discussion of the fundamental quantum mechanics may be found in Clayton 1983. The bound–bound cross section as a function of frequency is

$$\sigma(\omega)=\frac{4\pi^2\alpha}{M^2\omega_{ks}}\left|\langle k|\exp\left(i\frac{\omega_{ks}}{c}\boldsymbol{n}\cdot\boldsymbol{r}\right)\boldsymbol{\pi}\cdot\boldsymbol{\varepsilon}|s\rangle\right|^2\mathscr{L}(\omega-\omega_{ks}), \tag{20}$$

where $\hbar\omega_{ks}$ is the energy difference between the k and s states; s is the initial state; k is the final state; α is the fine structure constant, $\alpha\approx1/137$; $\boldsymbol{n}$ is the unit vector in the propagation direction of the photon; $\boldsymbol{\pi}=\boldsymbol{p}+(e/c)\boldsymbol{A}$; $\boldsymbol{\varepsilon}$ is the polarization vector of the photon, and $\mathscr{L}$ is the Lorentz profile,

$$\mathscr{L}(\omega-\omega_{ks})=\frac{\Gamma/2\pi}{(\omega-\omega_{ks})^2+(\Gamma/2)^2}, \tag{21}$$

where

$$\Gamma=\frac{2e^2\omega_{ks}^2}{3mc^3}f_{ks}, \tag{22}$$

and f_{ks} is the oscillator strength.

For the frequencies that dominate the opacities of cool neutron stars $(T<10^6$ K), it is a good approximation to assume $\exp[i(\omega_{ks}/c)\boldsymbol{n}\cdot\boldsymbol{r}]\approx1$. For the hydrogen ground state at $B/B_0=1000$, the frequency of a bound–bound transition is less than

$\omega \approx 250$ eV$\approx 1.3\times10^{7}$ cm^{-1}, while the wavefunction has a length scale of $r \approx 15\hat{\rho} \approx 1.7\times10^{-9}$ cm, so that $\exp[i(\omega_{ks}/c)\,\boldsymbol{n}\cdot\boldsymbol{r}] \approx e^{i(0.02)} \approx 1$. The dipole approximation will be worse for helium and carbon, since the frequencies involved are higher, but even for carbon at $B/B_0 = 1000$, the exponent is only 0.05, so the dipole approximation is valid to within 5 per cent over the entire range of parameters considered.

Substituting $\exp[i(\omega_{ks}/c)\,\boldsymbol{n}\cdot\boldsymbol{r}] = 1$ in (20), using the identity

$$\boldsymbol{\pi} = \left[\frac{\pi^2}{2M}, \boldsymbol{r}\right]\frac{i}{\hbar} \tag{23}$$

and simplifying, we find that the integral of the cross section over the line width Γ is

$$\int_{\Gamma} \sigma(\omega)\,d\omega = 4\pi^2\alpha\omega_{ks} \sum_{i=+,-,z} |\langle k|\,\boldsymbol{r}\cdot\boldsymbol{\varepsilon}_i|s\rangle|^2\,\gamma_i, \tag{24}$$

where γ_i is the fraction of the light polarized in direction i.

To get an idea of the selection rules for polarization, we will look at the case of right circular polarization, $\boldsymbol{\varepsilon}_i = \boldsymbol{\varepsilon}_+$. Here we are defining 'right circular' with respect to the magnetic field, not $\boldsymbol{n}$. Thus, if the photon is propagating parallel to the field, the convention is as usual, whereas if the two are antiparallel, the convention is opposite to the one normally used.

$$\langle m'\nu'|\,\boldsymbol{r}\cdot\boldsymbol{\varepsilon}_+|m\nu\rangle = \int f_{m\nu}f_{m'\nu'}\,dzI, \tag{25}$$

where

$$I = \int -\frac{\rho e^{i\phi}}{\sqrt{2}}\,\Phi_{0m}(\rho,\phi)\,\Phi^{*}_{0m'}(\rho,\phi)\,\rho\,d\rho\,d\phi. \tag{26}$$

Substituting in (5) and integrating, we find that

$$I = -\sqrt{m}\,\delta(m'+1-m)\,\hat{\rho}, \tag{27}$$

(δ is the Dirac delta) so that the right circular polarization gives transitions with $\Delta m = -1$, $\Delta\nu =$ even. Similarly, the $-$(left circular) polarization gives transitions with $\Delta m = +1$, $\Delta\nu =$ even and the z polarization has $\Delta m = 0$, $\Delta\nu =$ odd.

Therefore, the explicit expression for the bound–bound cross section is

$$\sigma(\omega) = 4\pi^2\alpha\omega \sum_{m\nu\nu'}\left[\gamma_+\mathscr{L}(\varepsilon_{m\nu}+\omega-\varepsilon_{(m-1)\nu'})\,m\hat{\rho}^2\left|\int f_{m\nu}f_{(m-1)\nu'}\,dz\right|^2 + \gamma_-\mathscr{L}(\varepsilon_{m\nu}+\omega-\varepsilon_{(m+1)\nu'})(m+1)\hat{\rho}^2\left|\int f_{m\nu}f_{(m+1)\nu'}\,dz\right|^2\right.$$
$$\left. + \gamma_z\mathscr{L}(\varepsilon_{m\nu}+\omega-\varepsilon_{m\nu'})\left|\int f_{m\nu}f_{m\nu'}\,z\,dz\right|^2\right], \tag{28}$$

where $\varepsilon_{m\nu}$ is the energy of the $m\nu$ orbital. The bound–free, or ionization, cross section is similar, except that the cross section is

$$\sigma(\omega) = 4\pi^2\alpha\omega\,|\langle k|\,\boldsymbol{r}\cdot\boldsymbol{\varepsilon}|s\rangle|^2\,\frac{\Delta n}{\Delta\omega}, \tag{29}$$

where Δn is the number of eigenstates in a frequency interval $\Delta\omega$ about the kinetic energy $E_k = \hbar\omega - \varepsilon_{m\nu}$. For a particle in a one-dimensional box of length L (appropriate for photon energies $\hbar\omega \ll \hbar\omega_c$, so the electron remains in the $n = 0$ Landau state), we have

$$\Delta n(E) = \frac{L\,dp}{h} \tag{30}$$

or, using $p = \sqrt{2EM}$ and $dE = \hbar\,d\omega$, we get

$$\frac{\Delta n}{\Delta\omega} = \frac{L\sqrt{2M}}{2\pi\sqrt{E}}. \tag{31}$$

In this box the normalized free wavefunctions is $g(p,z)/\sqrt{L}$, where $g(p,z)$ is the free wavefunction for momentum p, determined from the Schrödinger equation

$$-\frac{\hbar^2}{2M}\nabla^2 g + Vg = Eg,$$

where V is the atomic potential, $E = p^2/2M$ and $g(p,z) \equiv \exp(ipz/\hbar)$ at infinity. Therefore, the bound–free cross section becomes

$$\sigma(\omega) = 2\pi\alpha\omega \sum_{m\nu} \Theta(\omega + \varepsilon_{m\nu}) \sqrt{\frac{M}{E}} \left[\gamma_+ m\hat{\rho}^2 \left|\int f_{m\nu} g(p,z)\, dz\right|^2 + \gamma_-(m+1)\hat{\rho}^2 \left|\int f_{m\nu} g(p,z)\, dz\right|^2 + \gamma_z \left|\int f_{m\nu} g(p,z)\, z\, dz\right|^2\right], \tag{32}$$

where Θ is the step function,

$$\begin{aligned} \Theta(x) &= 0 \quad \text{for} \quad x < 0, \\ &= 1 \quad \text{for} \quad x \geq 0, \end{aligned} \tag{33}$$

M is the mass of the electron, and E is the kinetic energy of the electron.

3 TESTS OF THE PROGRAM

3.1 Convergence

As indicated in Section 2.1, the program integrates using an integration box of length L and a number of grid points N. We have tested the program to determine if the value of the energy converges in a small number of iterations; if in the limit of large N the energy converges; and if in the limit of large L the energy converges. Fig. 1 shows that for hydrogen, given L and N, the energy converges rapidly. In all of the cases tested, the energy varies by less than 0.01 eV after the third iteration. Next, in Fig. 2, the dependence of final energy on N with L constant is shown. Because of systematic integration error, the magnitude of the energy decreases with decreasing N for $\nu = 0$ or 2, while for $\nu = 1$ it increases with decreasing N. Finally, in Fig. 3, the energy as a function of L with N constant is shown. Since for $\nu \neq 0$ the wavefunction can extend past $L = 100\hat{\rho}$, there is significant error in the $\nu = 1$ and 2 energies, especially for high B. In all of the graphs, the ground state 000 is shown, since it is most perturbed by the Coulomb attraction; the excited states converge even more rapidly.

3.2 Comparison with previous results

Using a highly accurate multiconfigurational Hartree–Fock code, Rösner *et al.* (1984) and Forster *et al.* (1984) produced energies and transition strengths for hydrogen in arbitrary magnetic fields. The difference between the calculations in the above papers and those in the present one is that while the former considered mixing of states with $n > 0$, we restricted n to be 0. We did this in the interest of simplicity, as the inclusion of $n \neq 0$ states would considerably increase the difficulty of evaluating equation (9) and prevents us from studying the astrophysically interesting elements with $Z > 2$. More accurate computations will, however, have to take the mixing into account. Liu & Starace (1987) produced upper and lower bounds on the energy levels of hydrogen using a single-configuration method. While this is an excellent method for estimating the energies of hydrogenic elements, it is unfortunately difficult to generalize to $Z > 1$ because of the effects of electron–electron interactions. We emphasize that results for hydrogen presented below were generated only for comparison purposes, to give an idea of the magnitude of errors expected in our calculations for elements with $Z > 1$. Thus, our calculations for hydrogen are not as accurate as the most accurate previous work, and for detailed computations involving hydrogen, the work of Rösner *et al.* and Forster *et al.* is to be preferred. Table 1 shows the comparison between the high-field energy values of Rösner *et al.* 1984 and the values found in this paper. The largest difference in E, 3.4 per cent, occurs for the 000 state at $B/B_0 = 10$, as might be expected, since the lower the field and the more centrally condensed about the spherical nuclear potential the state, the less accurate is the (cylindrical) assumption that $n = 0$. In Table M1 (MN 253/1), the first table in the microfiche section †, we give the oscillator strengths for different transitions and compare them to the values given in Forster *et al.* 1984. The accuracy of the strengths of the transitions in which $\Delta m = 1$ is less than the accuracy of those for which $\Delta m = 0$, but even for $\Delta m = 1$ there are only two transitions for which the discrepancy in A is greater than 20 per cent. As was shown in Wunner, Ruder & Herold 1980, transitions with $\Delta m = 1$ will be affected by finite proton mass, which affects the energy levels of states with different m. However, since this effect is proportional to the cyclotron frequency of the nucleus, it will be less important for helium and carbon. In Table 2, our results for the ground-state binding

†This defines the convention we follow throughout this paper: Tables Mn ($n = 1, 2, \ldots, 20$) are to be found in the microfiche section. All other tables are included here in the main body of the paper. Table 5 in the main paper gives a summary of the contents of the microfiche tables.

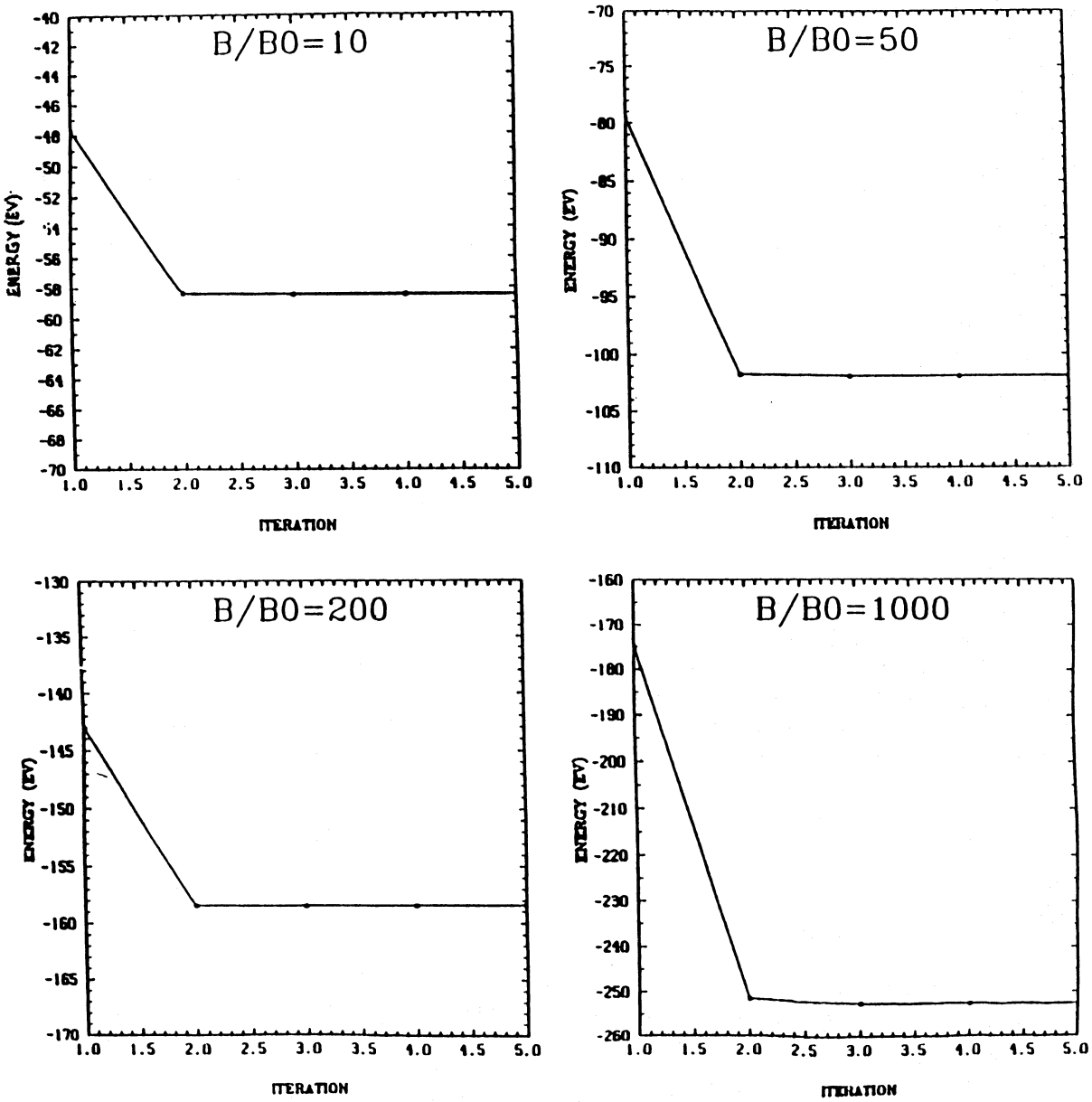

Figure 1. Convergence of hydrogen ground-state energy as a function of the number of iterations of the Hartree–Fock algorithm. The number of grid points is $N=2048$, and the integration box extends out to $L=800\hat{\rho}$. The magnetic field is in units of $B_0=4.7\times10^9$ G.

energies of helium in fields ranging from 2×10^{10} to 5×10^{13} G are compared with those of Pröschel *et al.* (1982). Here again we see a close correspondence, with by far the greatest difference (1.9 per cent) coming at $B=5\times10^{13}$ G. The reason for this difference is that [as we can see from (16) combined with (1)], the higher B is, the greater l is in units of $\hat{\rho}$, so that the contribution from the ends of the grid becomes more important. Table M2 (MN 253/1) shows the bound–free oscillator strengths A from the ground state of hydrogen. It is apparent that the higher the field, the more important are bound–free transitions. This is because as the field increases, the ground-state energy decreases logarithmically, while the energies of the other states stay roughly constant, so that the bound–bound transition energies become more nearly equal to each other and to the ionization energy, and as a result they become closer in transition strength as well. Therefore, transitions to highly excited states and bound–free transitions become relatively more important. Another test is that the oscillator strengths should obey the Thomas–Rieche–Kuhn sum rule. That is from a given initial state s of an electron,

$$\sum_k f_{ks}=1, \qquad (36),$$

where the sum is over all final states. Therefore, for an atom with Z electrons, the sum of the oscillator strengths of one-electron transitions will be Z. In Table M3 (MN 253/1) we list the sum of the bound–free and the first few bound–bound oscillator

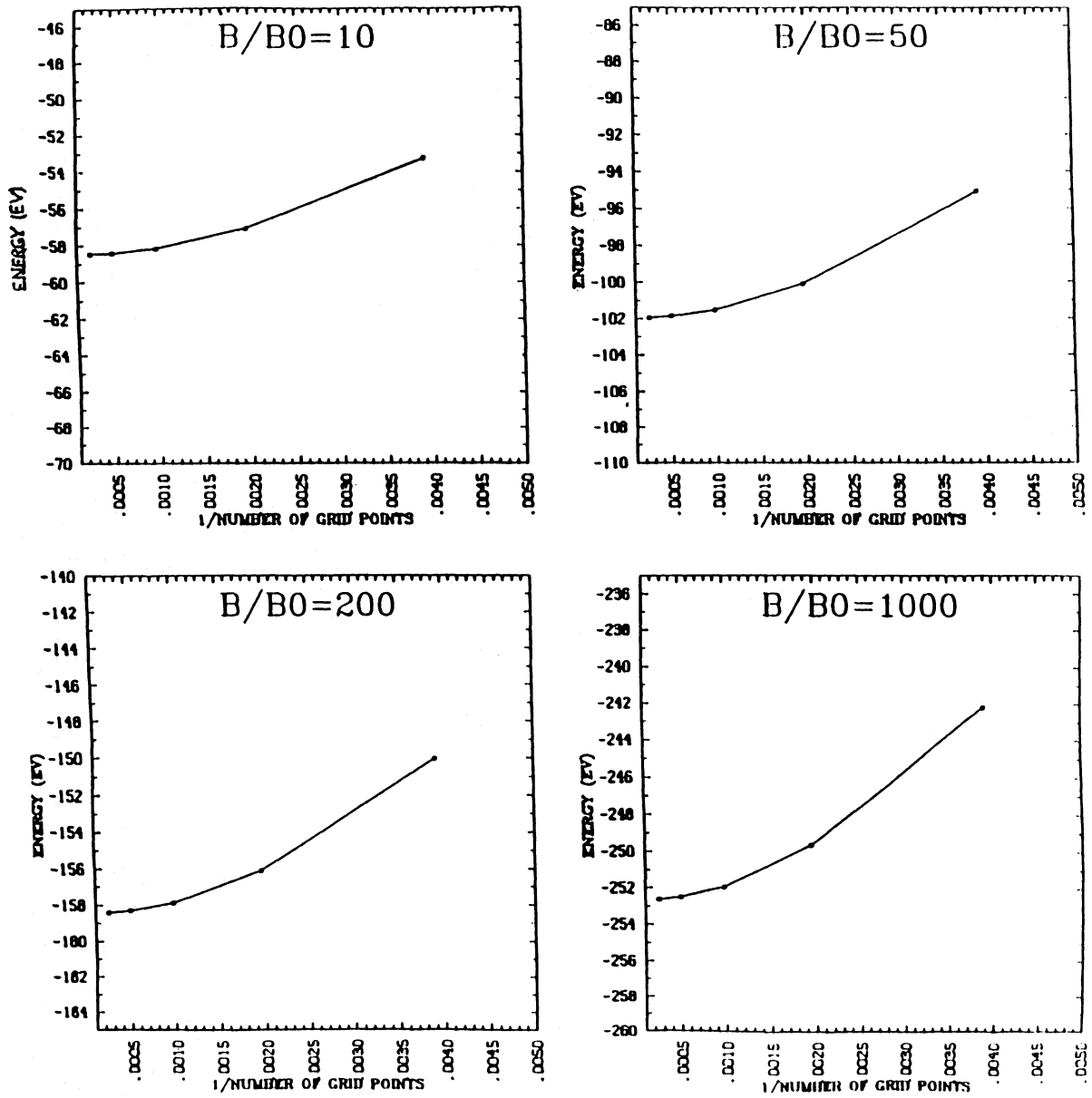

Figure 2. Final energy (after five iterations) of hydrogen ground state, with the number of grid points N varying and the size of the integration box held constant at $400\hat{\rho}$. The magnetic field is in units of $B_0 = 4.7 \times 10^9$ G.

strengths for hydrogen as a function of magnetic field. Clearly, while individual transition strengths to highly excited states might be small, their contribution as a whole is important, especially for high fields.

3.3 Error analysis for $Z > 1$

We find empirically that most of the differences between our computations for hydrogen and helium and previous adiabatic calculations can be removed by increasing the resolution and size of the grid. A determination of the scaling of these two types of error with Z will allow us to predict the errors in helium, carbon, etc. from those in hydrogen. The errors that are due to grid resolution can be estimated as follows. The integrations in (9) can be thought of as performed using Simpson's rule, so that the error in an integral of the form

$$\int_b^a h(z)\, dz,$$

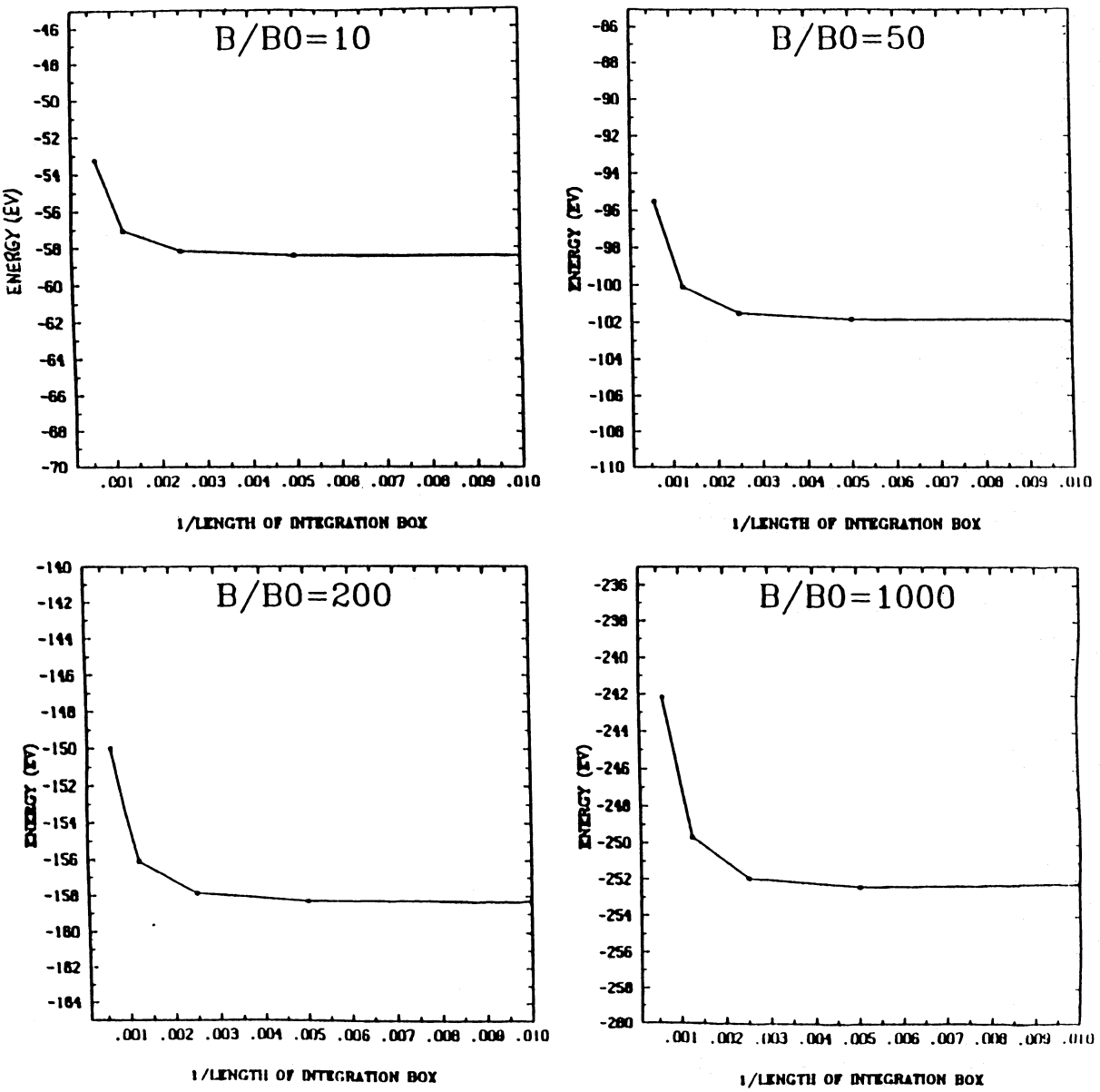

Figure 3. Final energy (after five iterations) of hydrogen ground state, with the size of the integration box L varying and the number of grid points held constant at 1024. The magnetic field is in units of $B_0 = 4.7 \times 10^9$ G, and L is in units of $\hat{\rho} = \sqrt{\hbar c/eB}$.

Table 1. Energies for hydrogen in several magnetic fields, in units of eV. The states are listed by their m and ν quantum numbers, with $n = 0$ assumed. The energies in parentheses are from the much more accurate tables of Rösner *et al.* and are to be preferred over ours for calculations requiring great precision. Our calculations are, however, more than accurate enough for the computation of neutron star thermal spectra. The number of grid points is $N = 2048$, and the integration box extends out to $L = 800\hat{\rho}$.

	B/B_0							
$m\nu$	10	20	30	50	100	200	500	1000
00	58.2	74.3	85.5	101.5	127.2	157.9	207.2	251.9
	(60.26)	(76.19)	(87.18)	(103.0)	(128.6)	(159.2)	(208.4)	(253.1)
01	11.24	11.93	12.27	12.61	12.96	13.18	13.34	13.35
	(11.25)	(11.93)	(12.27)	(12.61)	(12.96)	(13.21)	(13.40)	(13.48)
02	6.03	6.44	6.66	6.93	7.28	7.59	7.93	8.12
	(6.09)	(6.47)	(6.70)	(6.96)	(7.32)	(7.64)	(8.05)	(8.32)
10	39.5	51.3	59.5	71.4	90.8	114.5	153.3	189.0
	(39.7)	(51.6)	(59.8)	(71.7)	(91.0)	(114.7)	(153.4)	(189.1)
11	10.23	11.11	11.56	12.04	12.55	12.91	13.18	13.26
	(10.23)	(11.12)	(11.56)	(12.05)	(12.56)	(12.93)	(13.25)	(13.39)
12	5.39	5.83	6.07	6.37	6.74	7.09	7.48	7.69
	(5.41)	(5.84)	(6.09)	(6.39)	(6.77)	(7.14)	(7.59)	(7.90)

Table 2. Ground state energies for helium. The values in parentheses are from Pröschel *et al.* 1982. The number of grid points is $N=1024$, and the integration box extends out to $L=800\hat{\rho}$. The magnetic field is measured in Gauss, and the energy is given in electron volts.

B	E
2×10^{10}	137.42 (137.61)
5×10^{10}	196.47 (196.74)
1×10^{11}	255.23 (255.59)
2×10^{11}	328.97 (329.45)
5×10^{11}	454.28 (455.05)
1×10^{12}	575.14 (575.30)
2×10^{12}	719.27 (721.04)
5×10^{12}	955.74 (958.80)
1×10^{13}	1173.6 (1177.5)
2×10^{13}	1433.0 (1433.4)
5×10^{13}	1870.1 (1834.8)

with N steps, is

$$\delta \sim \frac{(b-a)^5}{N^4} h^{(4)}(\xi),$$

where ξ is some value between a and b. In an atom with $Z>1$, most of the error in energy will come from computing the energy of the innermost electron, as for this electron the Coulomb force has greater effect and consequently, the wave function is most concentrated at the origin and the effective grid resolution lowest. For this electron, the fourth derivative of the function $h(z)$ is of order

$$\frac{h(\xi)}{(z/\hat{\rho})^4},$$

evaluated at a characteristic value of z, $z=l$, where l is given by (16). Therefore, the error depends only on the ratio $l/\hat{\rho}$, not Z. Since for atomic number Z at magnetic field B this ratio is equal to that for hydrogen at magnetic field B/Z^2, we may estimate the error for higher atoms from the error for hydrogen at corresponding values of B/Z^2. For instance, for hydrogen at 2.35×10^{11} G, th ground-state energy estimate is 100.1 eV with 1024 grid points and an integration box of length $800\hat{\rho}$. With 2048 grid points and the same integration box, the estimate is 101.5 eV, for a difference of 1.4 per cent. For helium at $2.35\times10^{11}\times2^2=9.4\times10^{11}$ G, the correspoding difference is 5.4 eV/561.4 eV, or about 1.0 per cent. As another example, hydrogen at 1.41×10^{11} G has a difference of 0.4 eV out of a total of 85.5 eV (or about 0.5 per cent) between $N=2048$, $L=800\hat{\rho}$ and $N=4096$, $L=800\hat{\rho}$. Carbon at $1.41\times10^{11}\times6^2\approx4.7\times10^{12}$ G has a difference of 10 eV/1712 eV$\approx$0.6 per cent between calculations on those same grids. For excited states, the wavefunction is not as concentrated at the origin, so that it is not as important to have a finely spaced grid. In addition, for a neutral atom, excited states are influenced by an effective charge of $Z_{\rm eff}=1$ (because they are far away from the nucleus), so that excited state errors are roughly the same as the errors for the equivalent hydrogen states at the same magnetic field. We conclude that the technique of scaling from hydrogen allows us to make accurate estimates of the errors that are due to grid resolution for atoms with $Z>1$. Exactly the same argument may be applied to transition probabilities.

The magnitude of the second type of error, truncation of the integration box, may be estimated from equation (9) by noting that the size of the potential terms (which dominate over the kinetic term) is proportional to $|f_{m\nu}(z)|^2$. We find from experience that for states with $\nu=0$, it is necessary to extend the integration to $L=100\hat{\rho}$ for an accuracy of 0.1 per cent, while for excited states ($\nu>0$), $L=800\hat{\rho}$ may be required. This can necessitate a compromise, as in carbon in the (00, 10, 20, 30, 40, 51) state, where it is necessary to have both an extended integration box and a fine grid at the origin. Perhaps in future calculations an adaptive step size may take care of this problem.

The adiabatic calculations are exact only in the $B\rightarrow\infty$ limit, so it is also important to estimate the error that is due to assuming that $n=0$. This error is related to the ratio of Coulomb force to magnetic force, so that we may estimate the correction by comparing an atom with $Z>1$ at magnetic field B to the exact calculations of Rösner *et al.* for hydrogen at a field strength of B/Z^2. We have placed error estimates based on the above effects in the tables for helium and carbon. In general, the integration box is large enough that truncation errors contribute a negligible amount to the total error, while below $B/Z^2B_0=50$, non-adiabatic effects dominate and above $B/Z^2B_0=50$, grid resolution errors are the most important.

Table 3. Energy values for helium. The magnitude of the total energy is listed, as well as the energies of the individual orbitals, where E1 is the energy of the first orbital listed and E2 is the energy of the second orbital. Energies are given in electron volts. The estimated errors are in brackets, and are measured in eV. The number of grid points is $N=1024$, and the integration box extends out to $L=800\hat{\rho}$.

B/B_0	$m_1\nu_1, m_2\nu_2$	E_{tot}	E_1	E_2
50	00,10	343.0 [20]	173.4 [10]	95.69 [0.5]
	00,11	258.8 [16]	225.7 [14]	11.40 [0.01]
	00,12	254.1 [15]	236.0 [14]	6.64 [0.01]
	01,10	183.7 [0.9]	12.19 [0.01]	147.8 [0.7]
	02,10	178.8 [0.9]	7.26 [0.01]	158.8 [0.8]
	00,01	260.9 [16]	225.1 [14]	13.49 [0.01]
	00,02	255.1 [15]	235.0 [14]	7.65 [0.01]
	10,11	184.9 [1.0]	150.8 [0.8]	13.40 [0.01]
	10,12	178.6 [0.9]	160.4 [0.8]	7.06 [0.01]
200	00,10	556.0 [16]	274.7 [8]	156.2 [0.6]
	00,11	412.2 [12]	376.8 [11]	11.83 [0.01]
	00,12	407.8 [13]	387.3 [12]	7.39 [0.01]
	01,10	297.0 [1]	11.80 [0.01]	261.1 [1]
	02,10	293.1 [1]	7.92 [0.01]	271.0 [1]
	00,01	413.7 [12]	377.1 [11]	13.34 [0.01]
	00,02	408.8 [13]	386.5 [12]	8.41 [0.01]
	10,11	298.6 [1]	262.6 [1]	13.39 [0.01]
	10,12	293.1 [1]	272.5 [1]	7.87 [0.01]
1000	00,10	931.2 [19]	447.3 [9]	264.5 [0.5]
	00,11	680.4 [14]	643.9 [13]	11.97 [0.01]
	00,12	676.5 [14]	653.6 [13]	8.04 [0.01]
	01,10	503.5 [1.0]	11.65 [0.01]	467.6 [0.9]
	02,10	500.4 [1.0]	8.51 [0.01]	476.1 [0.9]
	00,01	681.5 [14]	644.7 [13]	13.08 [0.01]
	00,02	677.5 [14]	653.0 [13]	9.05 [0.01]
	10,11	504.9 [10]	468.5 [9]	13.09 [0.01]
	10,12	500.5 [11]	477.4 [10]	8.60[0.01]

4 RESULTS

The binding energies for a variety of states of helium in several field strengths are presented in Table 3. Also listed are the binding energies for the first and second orbitals. It can be seen that while the $\nu=0$ orbitals of hydrogen and helium are quite different in energy, the binding energies of the excited states are asymptotically equal (this is also true for the non-magnetic case, since the farther the electron is from the nucleus, the more the nucleus and inner $Z-1$ electrons look like a point charge of $Z=1$). Fig. 4 also illustrates this; when the state is tightly bound, the wavefunctions of hydrogen and helium differ significantly near the nucleus, while for loosely bound orbitals the wavefunctions are essentially identical. Table M4 (MN 253/1) gives the oscillator strengths from the helium ground state to several excited states. It can be seen that as with hydrogen, transitions to highly excited states become relatively more important for higher B. In Table 4 we give the binding energies of orbitals for carbon in magnetic fields of $B=200B_0$, $B=500B_0$ and $B=1000B_0$. In each case the ground-state energy of the whole atom is listed, along with the binding energies of various states. For the excited ($\nu\neq0$) states, all electrons other than the excited electron are assumed to be in their ground states. Again we see (Fig. 5) that while for the ground state the binding energies of carbon and hydrogen orbitals are radically different, for excited states they are very close. In Table M5 (MN 253/1) bound–bound oscillator strengths are listed, and in Table M6 (MN 253/1) bound–free oscillator strengths are given. These tables demonstrate that while bound–free transitions become weaker with increased field, the relative importance of the ionization process increases. In order to estimate the magnitude of errors in these computations, we calculated a few of the energies and oscillator strengths for helium and carbon with greater accuracy (i.e., more integration points). The result was that none of the energies changed by more than ~ 1 per cent, and none of the oscillator strengths changed by more than ~ 2 per cent.

In Tables M7 through M20 (MN 253/1), we give the energies and oscillator strengths of various ions of hydrogen, helium, carbon, nitrogen and silicon. To get a better quantitative idea of the magnitude of errors in these calculations, in the first part of Table M7 (MN 253/1) we compare our results for the energies of the ground state and the first excited state of hydrogen-like ions with the results of Rösner *et al.*, scaled appropriately. This scaling is given by

$$E_Z(B)=Z^2E_H(B/Z^2), \tag{37}$$

where $E_Z(B)$ is the energy of the hydrogenic atom with atomic number Z at magnetic field B and $E_H(B/Z^2)$ is the energy of hydrogen at magnetic field B/Z^2 (Rösner *et al.* 1984). In all cases the ground-state energies agree to within <10 per cent, and the excited-state energies agree within <1 per cent. As emphasized in the introduction, this accuracy is more than adequate for use in model atmosphere calculations for neutron stars, because the input parameters such as magnetic field and surface

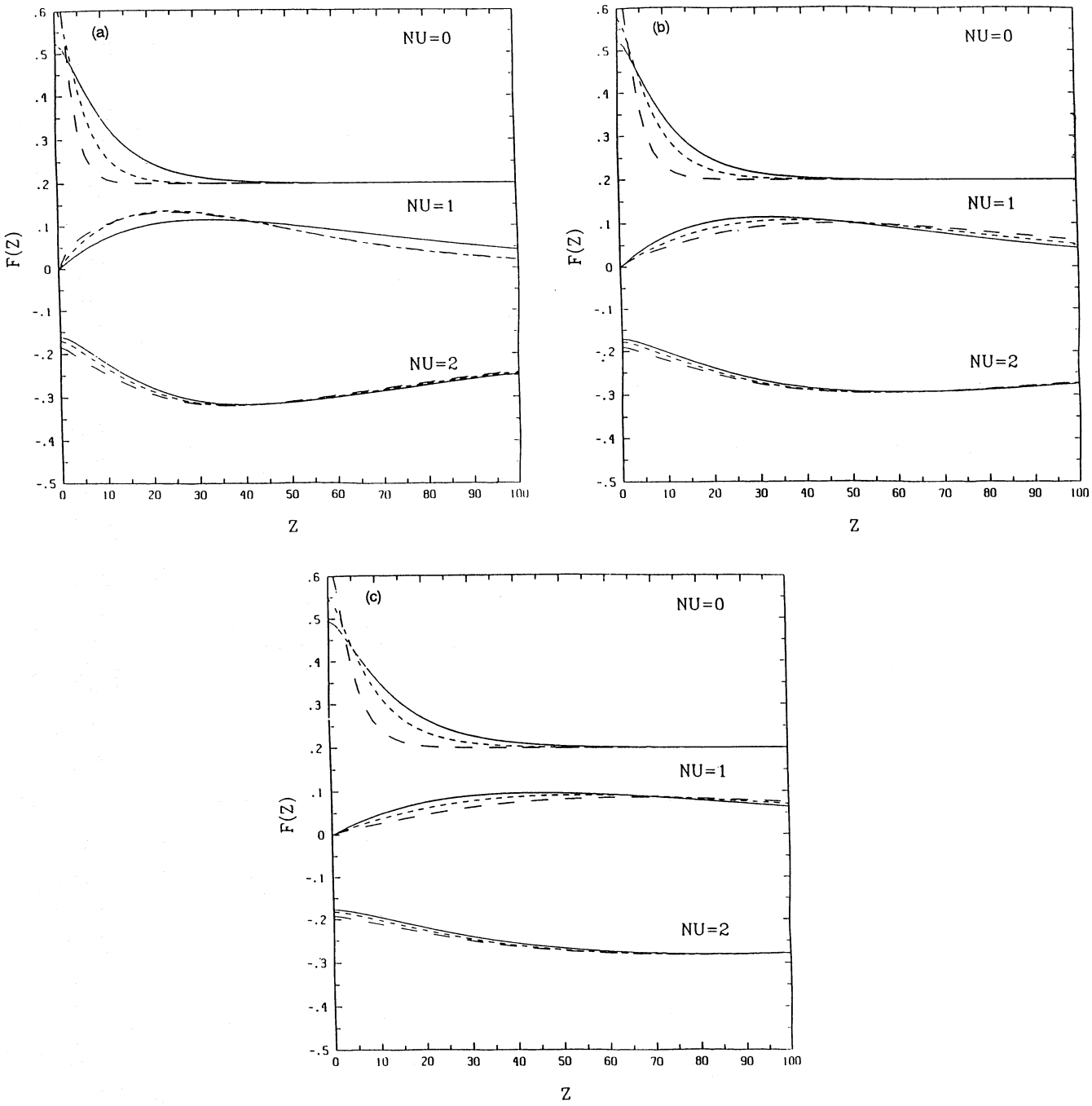

Figure 4. (a) Comparison of the z component of the wavefunction, $f_{m\nu}(z)$, for hydrogen, helium and carbon in a magnetic field of $B=200B_0=9.4\times10^{11}$ G. The solid line represents hydrogen, the short dashes represent helium, and the long dashes represent carbon. The graphs are labelled with the z quantum number, ν. (b) Comparison of the z component of the wavefunction, $f_{m\nu}(z)$, for hydrogen, helium and carbon in a magnetic field of $B=500B_0=2.35\times10^{12}$ G. The solid line represents hydrogen, the short dashes represent helium, and the long dashes represent carbon. The graphs are labelled with the z quantum number, ν. (c) Comparison of the z component of the wavefunction, $f_{m\nu}(z)$, for hydrogen, helium and carbon in a magnetic field of $B=1000B_0=4.7\times10^{12}$ G. The solid line represents hydrogen, the short dashes represent helium, and the long dashes represent carbon. The graphs are labelled with the z quantum number, ν.

temperature are more than 10 per cent uncertain. In the second part of Table M7 (MN 253/1) we give the values of the bound–free oscillator strengths from the ground states of hydrogenic ions and compare them with the extrapolation of our calculations for hydrogen. From Rösner *et al.* (1984) this scaling is

$$f(B,Z)=Z^0 f(B/Z^2,1). \tag{38}$$

Table M7 (MN 253/1) shows that the scaled oscillator strengths and directly computed oscillator strengths are consistent to within 20 per cent. As with the energies, this error is acceptable because it is overwhelmed by observational uncertainties and

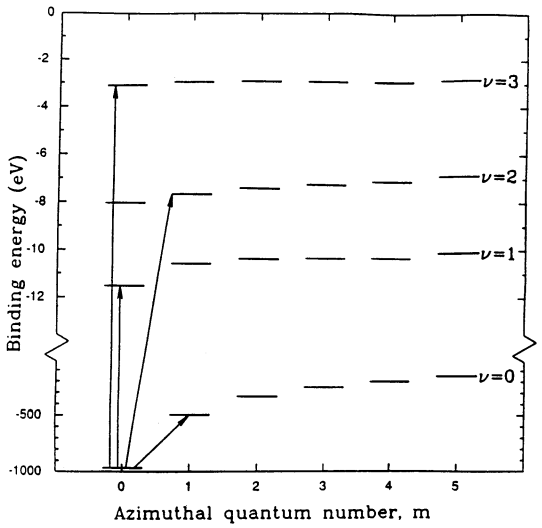

Figure 5. Energy levels and sample allowed transitions of carbon in a $B = 200B_0 = 9.4 \times 10^{11}$ G magnetic field. In this diagram, m and ν are taken to have the same meaning as in hydrogen, and where an excited state is drawn it is assumed that the other electrons are in their ground state (i.e., $\nu = 0$). The selection rule for transitions is that $\Delta m + \Delta \nu$ must be odd.

Table 4. Energies for carbon. The magnetic field is measured in units of $B_0 = 4.7 \times 10^9$ G, and when an excited state is listed, it is assumed that the other electrons are in their ground state (i.e., $\nu = 0$). The number of grid points is $N = 1024$, and the integration box extends out to $L = 800\hat{\rho}$, except for the ground state, which has $N = 512$ and $L = 100\hat{\rho}$. Energies are given in electron volts. The estimated errors are in brackets, and are measured in eV.

$B/B_0 = 200$
ground 4087.2

m	$\nu = 0$	$\nu = 1$	$\nu = 2$	$\nu = 3$
0	1011 [35]	11.522 [0.01]	8.047 [0.01]	3.101 [0.01]
1	499 [4]	10.575 [0.01]	7.652 [0.01]	2.945 [0.01]
2	331 [1]	10.361 [0.01]	7.414 [0.01]	2.907 [0.01]
3	247 [1]	10.316 [0.01]	7.236 [0.01]	2.897 [0.01]
4	193 [1]	10.290 [0.01]	7.074 [0.01]	2.891 [0.01]
5	144 [1]	10.089 [0.01]	6.858 [0.01]	2.854 [0.01]

$B/B_0 = 500$
ground 5783.7

m	$\nu = 0$	$\nu = 1$	$\nu = 2$	$\nu = 3$
0	1373 [40]	9.952 [0.01]	8.348 [0.01]	2.695 [0.01]
1	693 [3]	9.875 [0.01]	8.054 [0.01]	2.945 [0.01]
2	466 [1]	9.936 [0.01]	7.858 [0.01]	2.691 [0.01]
3	350 [1]	10.036 [0.01]	7.705 [0.01]	2.707 [0.01]
4	275 [1]	10.129 [0.01]	7.562 [0.01]	2.721 [0.01]
5	208 [1]	10.099 [0.01]	7.363 [0.01]	2.715 [0.01]

$B/B_0 = 1000$
ground 7448.4

m	$\nu = 0$	$\nu = 1$	$\nu = 2$	$\nu = 3$
0	1712 [35]	9.741 [0.01]	8.593 [0.01]	2.508 [0.01]
1	880 [3]	9.783 [0.01]	8.335 [0.01]	2.517 [0.01]
2	597 [1]	9.885 [0.01]	8.115 [0.01]	2.533 [0.01]
3	452 [1]	10.005 [0.01]	8.010 [0.01]	2.552 [0.01]
4	357 [1]	10.119 [0.01]	7.873 [0.01]	2.569 [0.01]
5	272 [1]	10.147 [0.01]	7.684 [0.01]	2.573 [0.01]

errors in the input parameters. In Tables M8 through M20 (MN 253/1), we present our results for ions with $Z > 1$. In these tables, it is understood that the energy or oscillator strength given for an electron in a state $(m\nu)$ is the energy or oscillator strength that that electron has when all other electrons are in their ground state.

These values are a step toward the construction of realistic model atmospheres for neutron stars. As we have stressed, the inevitable imprecision associated with observations of neutron star thermal spectra renders superfluous greater accuracy than is

Table 5. Contents of microfiche tables. In the tables all energies are in eV, and the reference magnetic field is $B_0 = 4.7 \times 10^9$ G.

Table M1. Oscillator strengths for hydrogen. The values in parentheses are from Forster *et al.* 1984. In the columns, the initial state is on the left and the final state is on the right.

Table M2. Bound–free oscillator strengths, f_{bf}, for hydrogen.

Table M3. Sum of oscillator strengths, Σf, for hydrogen. This table lists the sum of the transition strengths from the ground state, 00, to the excited states 01, 03, 10, 12 and the bound–free oscillator strength.

Table M4. Oscillator strengths for helium. In each case, the transition is from the ground state (00, 10) to the state listed. The estimated errors are in brackets.

Table M5. Bound–bound oscillator strengths for carbon. All transitions have their m value listed in Column 1, and the estimated errors are in brackets.

Table M6. Bound–free oscillator strengths for carbon.

Table M7. Binding energies and bound–free oscillator strengths for hydrogenic ions. The energies in parentheses are the extrapolated values of Rösner *et al.* 1984, and the oscillator strengths in parentheses are extrapolated from those of hydrogen as described in the text.

Tables M8–M20 list energies and bound–free oscillator strengths for atoms of atomic number Z in states with $m = 0$ to $z - 1$, where z is the number of electrons, and $\nu = 0, 1$ for:

Table M8. Helium-like ions of $Z = 2, 6, 7, 14$ for $B/B_0 = 200, 500, 1000$.
Table M9. Lithium-like ions of $Z = 6, 7, 14$ for $B/B_0 = 200, 500, 1000$.
Table M10. Beryllium-like ions of $Z = 6, 7, 14$ for $B/B_0 = 200, 500, 1000$.
Table M11. Boron-like ions of $Z = 6, 7, 14$ for $B/B_0 = 200, 500, 1000$.
Table M12. Carbon-like ions of $Z = 6, 7, 14$ for $B/B_0 = 200, 500, 1000$.
Table M13. Nitrogen for $B/B_0 = 200, 500, 1000$ and nitrogen-like silicon ($Z = 14$) for $B/B_0 = 1000$.
Table M14. Oxygen-like silicon for $B/B_0 = 1000$.
Table M15. Fluorine-like silicon for $B/B_0 = 1000$.
Table M16. Neon-like silicon for $B/B_0 = 1000$.
Table M17. Sodium-like silicon for $B/B_0 = 1000$.
Table M18. Magnesium-like silicon for $B/B_0 = 1000$.
Table M19. Aluminum-like silicon for $B/B_0 = 1000$.
Table M20. Neutral silicon for $B/B_0 = 1000$.

reported in this paper. Using the techniques in this paper, we have constructed opacity tables with various temperatures and surface compositions, and following Romani (1987) we have used (e.g. Mihalas 1978) techniques to calculate model atmospheres and spectra of emerging radiation. These computations are reported in a subsequent paper. We think that the accuracy of these calculations will be sufficient to make possible, for the first time, a reliable deduction of such essential parameters of neutron stars as the magnetic field, the surface temperature and the surface composition from the results of X-ray observations of these stars.

ACKNOWLEDGMENTS

We thank E. S. Phinney for proposing the problem, as well as for his guidance and many helpful suggestions. This work was supported in part by National Science Foundation grants AST84-51725 and PHY85-05682. MCM was partially supported by an NSF Graduate Fellowship.

REFERENCES

Alcock, C. & Illarionov, A., 1980. *Astrophys. J.*, **235,** 534.
Clayton, D., 1983. *Principles of Stellar Evolution and Nucleosynthesis,* The University of Chicago Press, Chicago.
Flowers, E. G., Lee, J. F., Ruderman, M. A., Sutherland, P. G., Hillbrandt, W. & Muller, E., 1977. *Astrophys. J.*, **215,** 291.
Forster, H., Strupat, W., Rösner, W., Wunner, G., Ruder, H. & Herold, H., 1984. *J. Phys. B: At. Mol. Phys.*, **17,** 1301.
Froese Fischer, C., 1977. *The Hartree–Fock Method for Atoms: A Numerical Approach,* Wiley, New York.
Hernquist, L., 1985. *PhD thesis,* California Institute of Technology.
Joss, P. C. & Rappaport, S. A., 1984. *Ann. Rev. Astr. Astrophys.*, **22,** 537.
Kara, S. M. & McDowell, M. R. C., 1980. *J. Phys. B: At. Mol. Phys.*, **13,** 1337.
Koonin, S. E., 1986. *Computational Physics,* p. 49, Benjamin/Cummings, Menlo Park, California.
Lee, J. F., 1976. *PhD thesis,* Columbia University.
Liebert, J., 1980. *Ann. Rev. Astr. Astrophys.*, **18,** 363.
Liu, C.-R. & Starace, A. F., 1987. *Phys. Rev. A,* **35,** 647.
Mihalas, D., 1978. *Stellar Atmospheres,* Freeman, San Francisco.
Miller, M. C., 1991. *Mon. Not. R. astr. Soc.*, submitted.
Neuhauser, D., 1986. *PhD thesis,* California Institute of Technology.
Neuhauser, D., Langanke, K. & Koonin, S. E., 1986. *Phys. Rev. A,* **33,** 2084.
O'Connell, R. F., 1979. *Phys. Lett.*, **70A,** 389.
Pratt, R. H., 1960. *Phys. Rev.*, **119,** 1619.

Pratt, R. H. & Tseng, H. K., 1972. *Phys. Rev. A,* **5,** 1063.
Pröschel, P., Rösner, W., Wunner, G., Ruder, H. & Herold, H., 1982. *J. Phys. B: At. Mol. Phys.,* **15,** 1959.
Romani, R. W., 1987. *Astrophys. J.,* **313,** 718.
Rösner, W., Herold, H., Ruder, H. & Wunner, G., 1983. *Phys. Rev. A,* **28,** 2071.
Rösner, W., Wunner, G., Herold, H. & Ruder, H., 1984. *J. Phys. B: At Mol. Phys.,* **17,** 29.
Ruder, H., Herold, H., Rösner, W. & Wunner, G., 1985. *Physica B and C,* **127,** 11.
Ruderman, M. A., 1971. *Phys. Rev. Lett.,* **27,** 1306.
Saloman, E. B., Hubbell, J. H. & Scofield, J. H., 1988. *At. Dat. Nuc. Dat. Tab.,* **38,** 1.
Shapiro, S. & Teukolsky, S., 1983. *Black Holes, White Dwarfs and Neutron Stars,* Wiley, New York.
Simola, J. & Virtamo, J., 1978. *J. Phys. B: At. Mol. Phys.,* **11,** 3309.
Taylor, J. H. & Stinebring, D. R., 1986. *Ann. Rev. Astr. Astrophys.,* **24,** 285.
Tsuruta, S., 1986. *Comm. Astrophys.,* **11,** 151.
Weissbluth, M., 1978. *Atoms and Molecules,* p. 400, Academic Press, New York.
Wunner, G., 1986. *J. Phys. B: At. Mol. Phys.,* **19,** 1623.
Wunner, G., Geyer, F. & Ruder, H., 1987. *Astrophys. Sp. Sci.,* **131,** 595.
Wunner, G. & Ruder, H., 1987. *Phys. Scr.,* **36,** 291.
Wunner, G., Ruder, H. & Herold, H., 1980. *Phys. Lett.,* **79A,** 159.
Wunner, G., Ruder, H. & Herold, H., 1981. *J. Phys. B: At. Mol. Phys.,* **14,** 765.

Monthly Notices
of the
ROYAL ASTRONOMICAL SOCIETY
Vol. 253 No. 1

Atoms in very strong magnetic fields

M. C. Miller and D. Neuhauser

Published for
The Royal Astronomical Society
by
Blackwell Scientific Publications
23 Ainslie Place
Edinburgh
EH3 6AJ

The microfiche are 105 x 148 mm archivally permanent silver halide film produced to internationally accepted standards in the NMA 98-image format

Microfiche produced by Micromedia, Bicester, Oxon

Microfiche Table Captions

In the tables all energies are in eV, and the reference magnetic field is $B_0 = 4.7 \times 10^9$G.

Table M1. Oscillator strengths for hydrogen. The values in parentheses are from Forster *et al.* 1984. In the columns, the initial state is on the left and the final state is on the right.

Table M2. Bound-free oscillator strengths, $f_{\rm bf}$, for hydrogen.

Table M3. Sum of oscillator strengths, $\sum f$, for hydrogen. This table lists the sum of the transition strengths from the ground state, 00, to the excited states 01, 03, 10, 12 and the bound-free oscillator strength.

Table M4. Oscillator strengths for helium. In each case, the transition is from the ground state (00,10) to the state listed. The estimated errors are in brackets.

Table M5. Bound-bound oscillator strengths for carbon. All transitions have their m-value listed in Column 1, and the estimated errors are in brackets.

Table M6. Bound-free oscillator strengths for carbon.

Table M7. Binding energies and bound-free oscillator strengths for hydrogenic ions. The energies in parentheses are the extrapolated values of Rosner et al. 1984, and the oscillator strengths in parentheses are extrapolated from those of hydrogen as described in the text.

Tables M8-M20 list energies and bound-free oscillator strengths for atoms of atomic number Z in states with $m = 0$ to $z - 1$, where z is the number of electrons, and $\nu = 0, 1$ for:

Table M8:helium-like ions of $Z = 2, 6, 7, 14$ for $B/B_0 = 200, 500, 1000$.

Table M9:lithium-like ions of $Z = 6, 7, 14$ for $B/B_0 = 200, 500, 1000$.

Table M10:beryllium-like ions of $Z = 6, 7, 14$ for $B/B_0 = 200, 500, 1000$.

Table M11:boron-like ions of $Z = 6, 7, 14$ for $B/B_0 = 200, 500, 1000$.

Table M12:carbon-like ions of $Z = 6, 7, 14$ for $B/B_0 = 200, 500, 1000$.

Table M13:nitrogen for $B/B_0 = 200, 500, 1000$ and nitrogen-like silicon ($Z = 14$) for B/B_0=1000.

Table M14:oxygen-like silicon for $B/B_0 = 1000$.

Table M15:fluorine-like silicon for $B/B_0 = 1000$.

Table M16:neon-like silicon for $B/B_0 = 1000$.

Table M17:sodium-like silicon for $B/B_0 = 1000$.

Table M18:magnesium-like silicon for $B/B_0 = 1000$.

Table M19:aluminum-like silicon for $B/B_0 = 1000$.

Table M20:neutral silicon for $B/B_0 = 1000$.

Table M1

B/B_0	$00 \rightarrow 01$	$01 \rightarrow 02$	$10 \rightarrow 00$	$12 \rightarrow 00$
10	0.553 (0.560)	1.426 (1.477)	6.706(−2) (6.876(−2))	8.757(−4) (8.206(−4))
20	0.488 (0.499)	1.387 (1.435)	4.137(−2) (4.328(−2))	4.132(−4) (4.010(−4))
30	0.449 (0.461)	1.365 (1.409)	3.123(−2) (3.284(−2))	2.645(−4) (2.604(−4))
50	0.402 (0.413)	1.331 (1.376)	2.174(−2) (2.317(−2))	1.491(−4) (1.496(−4))
100	0.340 (0.351)	1.284 (1.327)	1.318(−2) (1.444(−2))	6.790(−5) (6.949(−5))
200	0.284 (0.293)	1.234 (1.274)	7.871(−3) (9.062(−3))	3.052(−5) (3.196(−5))
500	0.219 (0.227)	1.173 (1.201)	3.919(−3) (5.055(−3))	1.047(−5) (1.142(−5))
1000	0.179 (0.186)	1.126 (1.144)	2.290(−3) (3.398(−3))	4.613(−6) (5.295(−6))

Table M2

B/B_0	f_{bf}
10	0.150
20	0.184
30	0.199
50	0.224
100	0.264
200	0.293
500	0.341
1000	0.374

Table M3

B/B_0	$\sum f$
10	0.770
20	0.673
30	0.679
50	0.648
100	0.617
200	0.585
500	0.564
1000	0.555

Table M4

B/B_0	01,10	00,11	03,10	00,13	00,02	10,12
50	0.206[5(-3)]	0.381[1(-2)]	2.74(-2)[5(-4)]	4.27(-2)[8(-4)]	3.56(-4)[2(-5)]	1.36(-3)[1(-4)]
200	0.113[3(-3)]	0.235[6(-3)]	1.51(-2)[4(-4)]	2.80(-2)[7(-4)]	1.66(-4)[4(-6)]	2.94(-4)[1(-6)]
1000	5.58(-2)[2(-3)]	0.125[5(-3)]	1.07(-2)[3(-4)]	1.99(-2)[6(-4)]	2.42(-5)[1(-6)]	4.84(-5)[3(-6)]

Table M5

$B/B_0 = 200$

m	$m0 \rightarrow m1$	$m0 \rightarrow m3$	$m1 \rightarrow m2$
0	3.969(-2)[1(-3)]	6.19(-3)[2(-4)]	0.94295[0.03]
1	5.672(-2)[2(-3)]	9.16(-3)[3(-4)]	0.94519[0.03]
2	7.996(-2)[2(-3)]	1.283(-2)[4(-4)]	1.01724[0.03]
3	0.10893[3(-3)]	1.716(-2)[6(-4)]	1.09588[0.03]
4	0.14450[3(-3)]	2.216(-2)[7(-4)]	1.15936[0.04]
5	0.19306[5(-3)]	2.817(-2)[9(-4)]	1.17476[0.04]

$B/B_0 = 500$

m	$m0 \rightarrow m1$	$m0 \rightarrow m3$	$m1 \rightarrow m2$
0	1.108(-2)[2(-4)]	1.79(-3)[6(-5)]	0.52859[0.02]
1	2.307(-2)[4(-4)]	3.68(-3)[1(-4)]	0.62992[0.02]
2	3.804(-2)[8(-4)]	5.97(-3)[2(-4)]	0.73442[0.02]
3	5.646(-2)[1(-3)]	8.68(-3)[3(-4)]	0.83148[0.03]
4	7.943(-2)[2(-3)]	1.191(-2)[4(-4)]	0.91552[0.03]
5	0.11250[2(-3)]	1.622(-2)[6(-4)]	0.97148[0.03]

$B/B_0 = 1000$

m	$m0 \rightarrow m1$	$m0 \rightarrow m3$	$m1 \rightarrow m2$
0	5.71(-3)[2(-4)]	8.9(-4)[4(-5)]	0.37876[0.01]
1	1.353(-2)[3(-4)]	2.08(-3)[1(-4)]	0.49172[0.02]
2	2.362(-2)[6(-4)]	3.56(-3)[2(-4)]	0.59544[0.02]
3	3.619(-2)[9(-4)]	5.36(-3)[3(-4)]	0.69025[0.02]
4	5.205(-2)[1(-3)]	7.55(-3)[4(-4)]	0.77605[0.03]
5	7.553(-2)[2(-3)]	1.061(-2)[5(-4)]	0.84587[0.03]

Table M6

$B/B_0 = 200$

$m\nu$	A
00	0.485
10	0.463
20	0.453
30	0.447
40	0.481
50	0.478

$B/B_0 = 500$

$m\nu$	A
00	0.429
10	0.419
20	0.423
30	0.427
40	0.431
50	0.411

$B/B_0 = 1000$

$m\nu$	A
00	0.399
10	0.400
20	0.399
30	0.397
40	0.403
50	0.405

Table M7

Energies

B/B0=200

Z	m	$\nu = 0$	$\nu = 1$
1	0	158(159)	13(13)
2	0	408(412)	52(50)
6	0	1653(1773)	382(378)
7	0	2050(2162)	496(494)

B/B0=500

Z	m	$\nu = 0$	$\nu = 1$
1	0	208(208)	13(13)
2	0	546(545)	52(52)
6	0	2313(2393)	419(415)
7	0	2871(2968)	552(552)

B/B0=1000

Z	m	$\nu = 0$	$\nu = 1$
1	0	252(253)	13(13)
2	0	676(670)	53(53)
6	0	2850(3051)	439(439)
7	0	3669(3754)	586(585)
14	0	8714(9367)	2060(2038)

Oscillator strengths

B/B0=200

Z	m	$\nu = 0$
1	0	0.28(0.29)
2	0	0.19(0.22)
6	0	0.10
7	0	0.11

B/B0=500

Z	m	$\nu = 0$
1	0	0.33(0.34)
2	0	0.25(0.27)
6	0	0.13(0.16)
7	0	0.13(0.15)

B/B0=1000

Z	m	$\nu = 0$
1	0	0.37(0.37)
2	0	0.30(0.30)
6	0	0.17(0.20)
7	0	0.14(0.18)
14	0	0.03

Table M8

B/B0=200

Z	Energies m	$\nu = 0$	$\nu = 1$	Oscillator strengths $\nu = 0$
2	0	271	12	0.49
	1	156	12	0.37
6	0	1500	290	0.12
	1	962	246	0.09
7	0	1870	380	0.13
	1	1194	338	0.09

B/B0=500

Z	Energies m	$\nu = 0$	$\nu = 1$	Oscillator strengths $\nu = 0$
2	0	365	12	0.47
	1	212	13	0.37
6	0	2060	290	0.20
	1	1366	275	0.12
7	0	2622	420	0.16
	1	1701	382	0.12

B/B0=1000

Z	Energies m	$\nu = 0$	$\nu = 1$	Oscillator strengths $\nu = 0$
2	0	447	12	0.55
	1	265	14	0.45
6	0	2580	310	0.21
	1	1800	240	0.15
7	0	3363	460	0.17
	1	2202	408	0.14
14	0	8312	1800	0.03
	1	5570	1601	0.06

Table M9

B/B0=200

	Energies			Oscillator strengths
Z	m	$\nu = 0$	$\nu = 1$	$\nu = 0$
6	0	1335	200	0.15
	1	838	170	0.11
	2	637	157	0.09
7	0	1686	290	0.16
	1	1073	260	0.11
	2	816	232	0.08

B/B0=500

	Energies			Oscillator strengths
Z	m	$\nu = 0$	$\nu = 0$	$\nu = 0$
6	0	1949	200	0.23
	1	1182	180	0.20
	2	909	173	0.18
7	0	2374	290	0.19
	1	1517	280	0.15
	2	1170	261	0.12

B/B0=1000

	Energies			Oscillator strengths
Z	m	$\nu = 0$	$\nu = 1$	$\nu = 0$
6	0	2400	200	0.25
	1	1500	180	0.22
	2	1150	180	0.19
7	0	3034	310	0.20
	1	1954	290	0.17
	2	1523	278	0.15
14	0	8022	1650	0.05
	1	5225	1350	0.06
	2	4200	1298	0.06

Table M10

B/B0=200

	Energies			Oscillator strengths
Z	m	$\nu = 0$	$\nu = 1$	$\nu = 0$
6	0	1287	115	0.22
	1	715	105	0.17
	2	534	95	0.14
	3	425	91	0.13
7	0	1568	200	0.20
	1	939	180	0.13
	2	713	165	0.11
	3	574	151	0.10

B/B0=500

	Energies			Oscillator strengths
Z	m	$\nu = 0$	$\nu = 1$	$\nu = 0$
6	0	1637	105	0.28
	1	1003	105	0.22
	2	765	105	0.19
	3	609	98	0.18
7	0	2176	200	0.23
	1	1319	180	0.18
	2	1020	180	0.15
	3	827	168	0.17

B/B0=1000

	Energies			Oscillator strengths
Z	m	$\nu = 0$	$\nu = 1$	$\nu = 0$
6	0	2005	105	0.40
	1	1255	105	0.31
	2	955	105	0.27
	3	800	100	0.22
7	0	2757	200	0.25
	1	1696	180	0.24
	2	1316	180	0.18
	3	1080	173	0.18
14	0	7601	1350	0.05
	1	5013	1250	0.08
	2	3979	1150	0.07
	3	3354	1065	0.05

Table M11

B/B0=200

	Energies			Oscillator strengths
Z	m	$\nu = 0$	$\nu = 1$	$\nu = 0$
6	0	1064	53	0.30
	1	592	45	0.26
	2	427	44	0.26
	3	338	44	0.21
	4	268	42	0.20
7	0	1442	125	0.20
	1	810	105	0.20
	2	595	95	0.17
	3	485	95	0.14
	4	397	89	0.13

B/B0=500

	Energies			Oscillator strengths
Z	m	$\nu = 0$	$\nu = 1$	$\nu = 0$
6	0	1460	45	0.36
	1	831	45	0.33
	2	604	45	0.34
	3	479	43	0.28
	4	385	45	0.27
7	0	1987	115	0.29
	1	1144	105	0.26
	2	855	105	0.22
	3	692	98	0.19
	4	573	97	0.23

B/B0=1000

	Energies			Oscillator strengths
Z	m	$\nu = 0$	$\nu = 1$	$\nu = 0$
6	0	1850	43	0.49
	1	1050	43	0.46
	2	810	42	0.38
	3	600	42	0.42
	4	500	40	0.32
7	0	2503	105	0.31
	1	1470	105	0.30
	2	1106	105	0.26
	3	897	95	0.26
	4	749	99	0.23
14	0	7396	1250	0.08
	1	4707	1050	0.11
	2	3683	950	0.08
	3	3178	950	0.07
	4	2746	872	0.08

Table M12

B/B0=200

		Energies		Oscillator strengths
Z	m	$\nu = 0$	$\nu = 1$	$nu = 0$
6	0	1011	12	0.42
	1	499	11	0.48
	2	331	10	0.60
	3	247	10	0.46
	4	193	10	0.44
	5	144	10	0.44
7	0	1278	60	0.28
	1	697	50	0.24
	2	490	45	0.25
	3	386	45	0.25
	4	316	42	0.23
	5	256	41	0.19

B/B0=500

		Energies		Oscillator strengths
Z	m	$\nu = 0$	$\nu = 1$	$\nu = 0$
6	0	1373	10	0.58
	1	693	10	0.63
	2	466	10	0.60
	3	350	10	0.57
	4	275	10	0.54
	5	208	10	0.51
7	0	1760	45	0.34
	1	977	45	0.40
	2	695	43	0.32
	3	549	43	0.33
	4	454	43	0.30
	5	371	44	0.25

B/B0=1000

		Energies		Oscillator strengths
Z	m	$\nu = 0$	$\nu = 1$	$\nu = 0$
6	0	1712	10	0.74
	1	880	10	0.74
	2	597	10	0.70
	3	452	10	0.68
	4	357	10	0.62
	5	272	10	0.56
7	0	2222	43	0.51
	1	1247	42	0 44
	2	896	42	0.48
	3	713	43	0.38
	4	592	43	0.35
	5	487	45	0.30
14	0	7106	1050	0.08
	1	4429	870	0.10
	2	3417	780	0.10
	3	2913	770	0.08
	4	2550	730	0.07
	5	2272	706	0.08

Table M13

B/B0=200

	Energies			Oscillator strengths
Z	m	$\nu = 0$	$\nu = 1$	$\nu = 0$
7	0	1190	10	0.45
	1	603	10	0.43
	2	398	10	0.46
	3	295	10	0.50
	4	232	10	0.42
	5	186	10	0.47
	6	142	10	0.41

B/B0=500

	Energies			Oscillator strengths
Z	m	$\nu = 0$	$\nu = 1$	$\nu = 0$
7	0	1635	10	0.48
	1	843	10	0.53
	2	562	10	0.66
	3	420	10	0.62
	4	332	10	0.51
	5	269	10	0.57
	6	207	10	0.59

B/B0=1000

	Energies			Oscillator strengths
Z	m	$\nu = 0$	$\nu = 1$	$\nu = 0$
7	0	2055	10	0.81
	1	1075	10	0.84
	2	724	10	0.72
	3	543	10	0.67
	4	433	10	0.69
	5	352	10	0.65
	6	273	10	0.59
14	0	6843	870	0.11
	1	4188	720	0.12
	2	3204	660	0.12
	3	2703	650	0.11
	4	2351	610	0.09
	5	2115	600	0.07
	6	1885	564	0.07

Table M14

Energies

B/B0=1000

Ground energy=30298

m	$\nu = 0$	$\nu = 1$
0	6629	730
1	3984	600
2	3006	550
3	2464	500
4	2155	500
5	1895	455
6	1727	455
7	1557	439

Oscillator strengths

B/B0=1000

m	$\nu = 0$
0	0.12
1	0.13
2	0.17
3	0.13
4	0.11
5	0.093
6	0.093
7	0.086

Table M15

Energies

B/B0=1000

Ground energy=31571

m	$\nu = 0$	$\nu = 1$
0	6381	550
1	3760	455
2	2791	420
3	2267	390
4	1949	380
5	1707	350
6	1540	340
7	1410	340
8	1273	330

Oscillator strengths

B/B0=1000

m	$\nu = 0$
0	0.12
1	0.16
2	0.14
3	0.15
4	0.13
5	0.13
6	0.14
7	0.12
8	0.098

Table M16

Energies

B/B0=1000

Ground energy=32595

m	$\nu = 0$	$\nu = 1$
0	6186	420
1	3568	340
2	2598	310
3	2070	280
4	1741	260
5	1531	260
6	1377	260
7	1238	240
8	1135	240
9	1024	236

Oscillator strengths

B/B0=1000

m	$\nu = 0$
0	0.16
1	0.20
2	0.18
3	0.20
4	0.16
5	0.17
6	0.16
7	0.15
8	0.14
9	0.12

Table M17

Energies

B/B0=1000

Ground energy=33396

m	$\nu = 0$	$\nu = 1$
0	5994	290
1	3372	220
2	2405	200
3	1882	180
4	1572	180
5	1351	170
6	1200	170
7	1085	170
8	991	170
9	893	155
10	801	155

Oscillator strengths

B/B0=1000

m	$\nu = 0$
0	0.17
1	0.20
2	0.23
3	0.30
4	0.28
5	0.20
6	0.18
7	0.20
8	0.19
9	0.18
10	0.17

Table M18

Energies

B/B0=1000

Ground energy=33998

m	$\nu = 0$	$\nu = 1$
0	5822	180
1	3198	125
2	2232	115
3	1715	105
4	1394	98
5	1180	95
6	1030	95
7	912	90
8	823	90
9	749	90
10	680	90
11	602	90

Oscillator strengths

B/B0=1000

m	$\nu =$
0	0.17
1	0.28
2	0.30
3	0.31
4	0.32
5	0.31
6	0.28
7	0.25
8	0.42
9	0.31
10	0.24
11	0.22

Table M19

Energies

B/B0=1000

Ground energy=34421

m	$\nu = 0$	$\nu = 1$
0	5656	80
1	3037	51
2	2065	45
3	1549	43
4	1235	43
5	1019	39
6	869	39
7	757	39
8	672	39
9	603	39
10	544	39
11	488	39
12	423	39

Oscillator strengths

B/B0=1000

m	$\nu = 0$
0	0.28
1	0.28
2	0.38
3	0.43
4	0.40
5	0.40
6	0.43
7	0.37
8	0.47
9	0.40
10	0.39
11	0.35
12	0.37

Table M20

Energies

B/B0=1000

Ground energy=34683

m	$\nu = 0$	$\nu = 1$
0	5502	13
1	2885	10
2	1911	9
3	1397	9
4	1080	9
5	868	9
6	718	9
7	609	9
8	525	9
9	460	9
10	407	9
11	360	9
12	314	9
13	262	9

Oscillator strengths

B/B0=1000

m	$\nu =$
0	0.28
1	0.45
2	0.44
3	0.71
4	0.53
5	0.73
6	0.74
7	0.85
8	0.66
9	0.81
10	0.69
11	0.60
12	0.69
13	0.60